Affinity selection and sequence-activity relationships of HIV-1 membrane fusion inhibitors directed at the drug-resistant variants†

Shinya Oishi,*[a] Kentaro Watanabe,[a] Saori Ito,[a] Michinori Tanaka,[a] Hiroki Nishikawa,[a] Hiroaki Ohno,[a] Kazuki Shimane,[b] Kazuki Izumi,[b] Yasuko Sakagami,[b] Eiichi N. Kodama,‡[b] Masao Matsuoka,[b] Akira Asai[c] and Nobutaka Fujii*[a]

Enfuvirtide is the first approved membrane fusion inhibitor against HIV-1. Although this drug is effective against multi-drug resistant strains, the emergence of enfuvirtide-resistant strains has been reported in patients who have received an enfuvirtide-containing regimen. Based on the high affinity of synthetic HIV-1 gp41 C-terminal heptad repeat (C-HR) peptides to the counterpart trimeric N-terminal heptad repeat (N-HR) coiled-coil structure, a novel screening approach has been established to facilitate the identification of potent fusion inhibitors against wild-type and enfuvirtide-resistant HIV-1. In this process, affinity selection using histidine-tagged N-HR peptides with the sequences derived from wild-type and resistant strains efficiently captured potent inhibitory peptides from a pool of highly water-soluble C-HR peptides with α-helix-inducible motifs. A highly potent peptide was found from a single amino acid substitution observed in an enfuvirtide-resistant variant as well as peptides with unprecedented modifications at the mutated site.

Introduction

Several inhibitors that block viral attachment and the fusion process have been approved for the treatment of human immunodeficiency virus (HIV) in the past decade. The first fusion inhibitor, enfuvirtide (T-20), binds to the N-terminal heptad repeat (N-HR) of the HIV-1 envelop glycoprotein gp41,[1] and prevents the formation of a fusogenic antiparallel coiled-coil structure (known as the six-helical bundle) between N-HR and the C-terminal heptad repeat (C-HR) (Fig. 1a).[2] Enfuvirtide is effective even against the clinical strains that are resistant to multiple drug classes such as reverse transcriptase inhibitors and protease inhibitors used in highly active antiretroviral therapy (HAART). However, the emergence of enfuvirtide-resistant strains has been reported in patients receiving long-term enfuvirtide treatment.[3,4]

The primary evolution of enfuvirtide resistance occurs on gp41 N-HR, which attenuates the binding affinity with enfuvirtide, resulting in decreased drug susceptibility.[3–5] The major primary mutations are V38A and N43D in the Leu33–Leu45 region of N-HR. These mutations subsequently lead to a secondary mutation appearing in C-HR, which can compensate the binding

affinity between viral N-HR and C-HR for efficient gp41 folding.[6] For example, N126K and S138A mutations have been reported to enhance the resistance induced by enfuvirtide and another inhibitory C-HR peptide, C34. These complementary mutations, which occur at the face-to-face positions of N-HR and C-HR verified by crystallographic studies,[7–9] can restore the critical step required for viral infection into the target cells and eliminate the inhibitory effect of exogenous enfuvirtide.
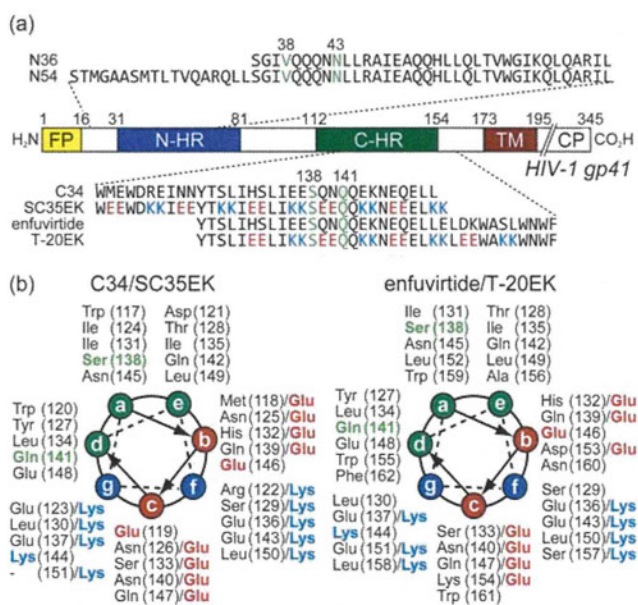

Fig. 1 HIV-1 envelope protein gp41 and the amino acid sequences. (a) Schematic representation of HIV-1 gp41. FP: fusion peptide; TM: transmembrane domain; CP: cytoplasmic tail. (b) Helical-wheel representation of C34/SC35EK and enfuvirtide/T-20EK.

[a] Graduate School of Pharmaceutical Sciences, Kyoto University, Sakyo-ku, Kyoto 606-8501, Japan. E-mail: soishi@pharm.kyoto-u.ac.jp; nfujii@pharm.kyoto-u.ac.jp; Fax: +81-75-753-4570; Tel: +81-75-753-4551

[b] Laboratory of Virus Control, Institute for Virus Research, Kyoto University, Sakyo-ku, Kyoto 606-8507, Japan

[c] Graduate School of Pharmaceutical Sciences, University of Shizuoka, Suruga-ku, Shizuoka 422-8526, Japan

† Electronic supplementary information (ESI) available: Additional experimental procedures, measurement of CD spectra, bioassays, and MS data. See DOI: 10.1039/c0md00091d

‡ Present address: Division of Emerging Infectious Diseases, Tohoku University School of Medicine, Sendai 980-8575, Japan

Recently, several novel fusion inhibitors such as tifuvirtide (T-1249)[10] and sifuvirtide,[11] which are effective against these enfuvirtide-resistant viruses, have been reported. We have also demonstrated a novel tailored design of fusion inhibitors based on the enfuvirtide-resistant mutation to preempt this escape strategy of HIV-1.[12] Enfuvirtide analogues carrying a substitution corresponding to the secondary mutation were found to exert potent anti-HIV activity against wild-type and enfuvirtide-resistant strains with the primary mutations. Of interest, during this observation, we found that enfuvirtide analogues with other substitutions were also effective against these strains. Alternatively, modification of a single residue in C-HR such as Q141L, which is involved in the increased syncytium-forming ability of the mutant virus,[13] led to an increase in the anti-HIV potency of inhibitor C34.[14] These observations implied that the C-HR sequence with substitutions, which were not spontaneously elaborated by single nucleotide mutations from wild-type HIV-1, could represent potent fusion inhibitors. Encouraged by these results, the optimization of interactive residues of fusion inhibitors against wild-type and enfuvirtide-resistant viruses was undertaken.

Affinity selection-mass spectrometry (AS-MS) is a promising methodology for compound screening, in which target molecule-bound components are captured from a pool of candidates and are identified by mass spectrometry. The successful applications of this technique are exemplified by the identification of kinase inhibitors[15] and antifungal natural products.[16] This simple selection process by virtue of the binding affinity can be a facile alternative to functional bioassays, although the functions and mechanisms of captured compounds for bioactivity cannot be determined. For medicinal chemistry of HIV fusion inhibitors, this approach should be suitable in the optimization of inhibitory C-HR peptides such as T-20EK[17] and SC35EK.[18] Taking advantage of the trimeric N-HR coiled-coil as a target molecule, a mixture of C-HR peptides with a single amino acid substitution can be screened without using recombinant or clinical HIV strains.[19,20] We envisioned that the competitive binding of C-HR components would capture relatively more potent anti-HIV peptides with higher affinity towards N-HR. Herein we report on the affinity-based screening technology and sequence-activity relationships for amino acid optimization in HIV-1 fusion inhibitors directed against enfuvirtide-resistant HIV strains.

Results and discussion

T-20EK and SC35EK are characterized by repeated X-EE-XX-KK motifs that stabilize the bioactive α-helix structure of enfuvirtide and C34, respectively (Fig. 1a). Potential electrostatic interactions between glutamic acid (Glu) and lysine (Lys) residues at i and $i + 4$ positions, respectively, are distinct from the traditional stabilization with stapled covalent linkages.[21,22] Consistent substitution of the residues located on the non-interactive surface of the C-HR α-helix with Glu or Lys achieved an enhancement in affinity toward the N-HR sequence and anti-HIV activity. This process disclosed the indispensable residues in C-HR for direct interaction with viral N-HR (Fig. 1b).[23] Additionally, in contrast to native sequences of C-HR peptides that are highly hydrophobic, substitution with charged amino acids markedly improved the aqueous solubility of the peptides.

This design allowed us to prepare a homogeneous mixture of the SC35EK derivatives and T-20EK derivatives at high concentrations.

Initially, C-HR peptide libraries with a variety of canonical amino acid substitutions at the positions to be optimized (Ser138 and Gln141) were prepared by a split-pool method. After the construction of the C-terminal sequence using a standard Fmoc-based solid-phase peptide synthesis approach, the resin was split into fractions at position 138 or 141, where proteinogenic amino acids except for cysteine were coupled in parallel. The 19 fractions were combined again and the N-terminal sequence was constructed in one portion. All the protected peptide resins were treated with a cocktail of deprotection reagents, and the crude peptides were purified by reversed-phase HPLC to afford the expected peptides.

Separately, in order to rationalize the selection process by affinity-based technology and to investigate the sequence-activity relationship, all C-HR peptides with a single substitution were prepared in parallel and were evaluated for the biological and physicochemical properties individually. The counterpart N-HR peptides of the wild-type and enfuvirtide-resistant variants (V38A and N43D) were also prepared. For affinity selection, the histidine tag (His$_6$) sequence of the N-HR peptides was attached on the N-terminus via an aminocaproic acid-glycine dipeptide linker. This linker was incorporated to avoid the possible disruption of N-HR and C-HR interaction by positively charged His$_6$-tag. Anti-HIV activities of all the C-HR peptides against laboratory wild-type HIV-1$_{NL4-3}$ or the variants with enfuvirtide-resistant mutations were evaluated using the MAGI assay. Thermal stabilities of the potential six-helical bundles consisting of N-HR and C-HR peptides were evaluated by measuring the melting temperature (T_m) using the molar ellipticity value at 222 nm in circular dichroic (CD) spectra of N36/SC35EK or N54/T-20EK mixture (Figure S1, ESI†).

The AS-MS protocol was optimized using SC35EK derivatives (Table 1). A pool of SC35EK$_{S138X}$ was incubated with a wild-type N-HR peptide, N36 (10 μM) with an N-terminal His$_6$-tag, in HEPES buffer (pH 7.4). The potential six-helical bundles of N36–SC35EK$_{S138X}$ were captured by Ni-NTA agarose resin and were subsequently eluted with 50% AcOH (Fig. 2a). The captured components were separated and characterized by LC-MS analysis, except that the peptides with Leu and Ile were observed as overlapping peaks of the same mass-to-charge ratio (Fig. 2b). The recovery rate in affinity selection for relative binding ability to N36 was calculated from the detected signal of $[M + 3H]^{3+}$ and $[M + 4H]^{4+}$ ions of each C-HR peptide by the LC-MS analysis of captured peptides. Under the high concentration conditions (10 μM each of SC35EK$_{S138X}$), several potent peptides including a resistant variant-derived S138A peptide were captured in high recovery rates, while slightly less potent peptides such as SC35EK$_{S138F}$ and SC35EK$_{S138Y}$ were not detected. In contrast, when the total concentration of the mixture was nearly equal to the N36 concentration (0.6 μM each of SC35EK$_{S138X}$), there was no discernible difference in the recovery rates of each peptide. The compound with the least potent anti-HIV activity in the series, SC35EK$_{S138R}$, was recovered under this equimolar concentration conditions. This recovery suggested that the method is not effective under lower concentration conditions of C-HR peptides. A condition using

This journal is © The Royal Society of Chemistry 2010

Med. Chem. Commun., 2010, 1, 276–281 | 277

Table 1 Optimization of the affinity selection protocol

X	Recovery (%)[a]					
	Concentration of SC35EK$_{S138X}$/μM					
	10	6	1	0.6	EC$_{50}$/nM[b]	T_m/°C[c]
Ser	22.8	19.2	11.5	5.8	1.0 ± 0.14	81.6
Ala	30.7	22.5	11.5	5.3	1.2 ± 0.12	86.4
Asp	0.7	0.0	0.0	4.3	15 ± 3.3	59.7
Glu	1.3	1.0	1.8	5.1	15 ± 0.69	66.2
Phe	0.7	0.6	4.0	6.3	1.5 ± 0.10	72.9
Gly	13.8	14.4	11.6	5.9	1.9 ± 0.26	79.1
His	0.9	0.6	2.4	5.7	1.9 ± 0.57	62.9
Ile	4.7[d]	7.6[d]	11.3[d]	6.9[d]	1.3 ± 0.54	84.6
Lys	0.2	0.1	0.0	3.6	8.2 ± 1.7	53.5
Leu	4.7[d]	7.6[d]	11.3[d]	6.9[d]	0.93 ± 0.16	83.2
Met	8.9	13.3	12.5	6.8	0.68 ± 0.06	84.1
Asn	1.1	0.5	4.3	6.4	2.2 ± 0.47	69.0
Pro	0.4	0.2	0.1	4.5	35 ± 9.2	56.1
Gln	0.9	0.5	2.1	6.1	2.4 ± 0.79	65.9
Arg	0.3	0.1	0.0	2.5	280 ± 47	52.3
Thr	9.0	12.8	11.7	5.7	1.8 ± 0.27	79.7
Val	2.8	6.0	12.1	7.0	1.9 ± 0.64	79.9
Trp	0.5	0.3	0.9	6.2	3.1 ± 0.52	66.4
Tyr	0.5	0.4	2.3	5.9	1.9 ± 0.71	68.0

[a] The recovery rate was determined from the relative detected signals of [M + 3H]$^{3+}$ and [M + 4H]$^{4+}$ ions by LC-MS analysis. [b] EC$_{50}$ was determined as the concentration that blocked HIV-1$_{NL4-3}$ replication by 50% in the MAGI assay. To improve the replication kinetics, the D36G mutation, observed in the majority of HIV-1 strains, was introduced into the NL4-3 background used in this study. [c] T_m values were defined by the midpoint of the thermal unfolding transition state measured by monitoring the molar ellipticity at 222 nm of N36/SC35EK$_{S138X}$ mixture. [d] Combined yield of 138I and 138L derivatives.

1 μM each of SC35EK$_{S138X}$ (total 19 μM of the mixture) for affinity selection was selected for further experiments, in which the recovery rate was found to positively correlate with the stability of the six-helical bundle (Fig. 3a). Although an ideal linear correlation was not observed between the logarithmic EC$_{50}$ of anti-HIV activity and the recovery rate (Fig. 3b), the peptides, which were captured in relatively high yields by affinity selection, exhibited highly potent anti-HIV activity.
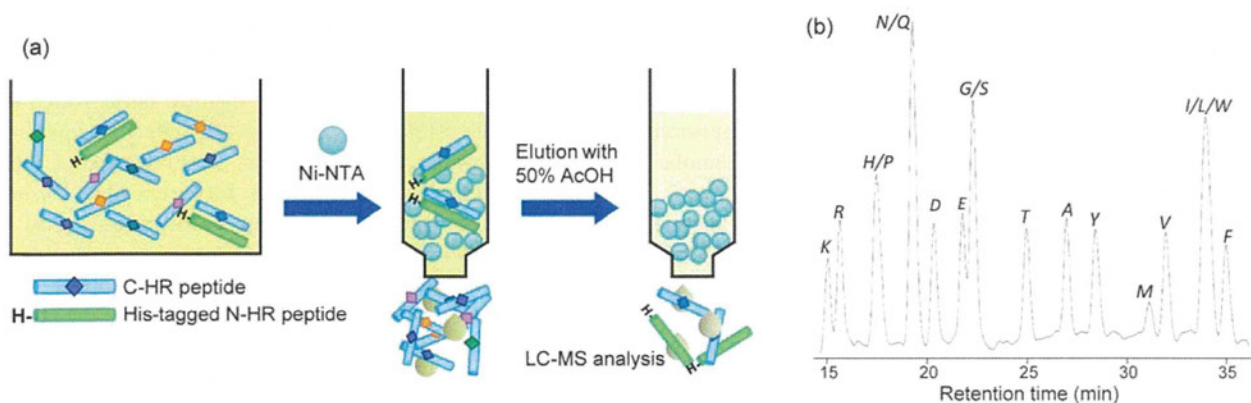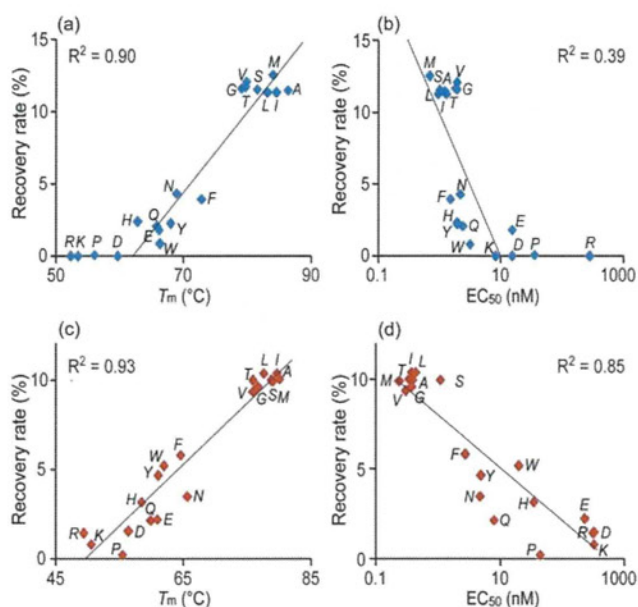

Fig. 3 Correlation between the recovery rate and the thermal stability, or the anti-HIV activity. (a, b) SC35EK$_{S138X}$; (c, d) T-20EK$_{S138X}$. R^2 values for the correlation of SC35EK$_{S138X}$ data were calculated without using the data points of S138R/K/P/D mutants ($n = 15$).

The optimized condition was applied for the selection of T-20EK$_{S138X}$ derivatives (Table 2). The anti-HIV activity of T-20EK$_{S138X}$ was found to be dependent on the amino acid type at position 138. Substitution with aliphatic side-chain amino acids such as Ala, Ile, Leu, Met and Val, displayed highly potent anti-HIV activity, although significant stabilization of the N54–T-20EK$_{S138X}$ complexes was not observed. Gly- and Thr-substitutions were also observed to increase potency. In contrast, hydrophilic, charged and aromatic amino acid substitutions at position 138 reduced binding with N54. In our previous study, it was demonstrated that higher affinity with the N-HR sequence and more potent anti-HIV activity of C34$_{S138A}$ and T-20$_{S138A}$ were due to the dominant contribution of larger desolvation free energy of the hydrophobic side-chain.[8] The structure–activity

Fig. 2 Affinity selection of the HIV-1 fusion inhibitors. (a) Protocol outlining the affinity selection of C-HR peptides using the histidine-tagged N-HR peptide. (b) HPLC profile of a pool of SC35EK derivatives with a single amino acid substitution at position 138 [Cosmosil 5C18 AR-II column; linear 30–40% MeCN gradient over 40 min; flow rate, 1 cm^3 min^{-1}; detection at 220 nm].

Table 2 Recovery rate in affinity selection and anti-HIV activity of T-20EK$_{S138X}$, and the thermal stability of the N54–T-20EK$_{S138X}$ complex

X	Recovery (%)[a]	EC$_{50}$/nM[b]	T_m/°C[c]	X	Recovery (%)[a]	EC$_{50}$/nM[b]	T_m/°C[c]
Ser	10.0	1.1 ± 0.2	78.8				
Ala	10.0	0.3 ± 0.1	80.1	Met	9.9	0.2 ± 0.1	79.0
Asp	1.5	330 ± 96	56.5	Asn	3.5	4.8 ± 1.6	65.7
Glu	2.2	230 ± 31	61.0	Pro	0.2	44 ± 8	55.5
Phe	5.8	2.8 ± 0.2	64.6	Gln	2.2	7.9 ± 3.4	60.0
Gly	9.6	0.4 ± 0.2	76.7	Arg	1.5	320 ± 88	49.4
His	3.2	35 ± 10	58.5	Thr	10.0	0.4 ± 0.2	75.9
Ile	10.4[d]	0.4 ± 0.1	79.7	Val	9.4	0.3 ± 0.1	76.0
Lys	0.8	330 ± 67	50.6	Trp	5.2	20 ± 9	62.0
Leu	10.4[d]	0.4 ± 0.3	77.6	Tyr	4.7	5.0 ± 1.5	61.1

[a] The recovery rate was determined from the relative detected signals of [M + 3H]$^{3+}$ and [M + 4H]$^{4+}$ ions by LC-MS analysis. [b] EC$_{50}$ was determined as the concentration that blocked HIV-1$_{NL4-3}$ replication by 50% in the MAGI assay. To improve the replication kinetics, the D36G mutation, observed in the majority of HIV-1 strains, was introduced into the NL4-3 background used in this study. [c] T_m values were defined by the midpoint of the thermal unfolding transition state measured by monitoring the molar ellipticity at 222 nm of N54/T-20EK$_{S138X}$ mixture. [d] Combined yield of 138I and 138L derivatives.

Table 3 Peptide recovery in affinity selection, anti-HIV activity and thermal stability of the six-helix bundles of C-HR peptides against enfuvirtide-resistant variants

X	SC35EK$_{S138X}$			T-20EK$_{S138X}$		
	Recovery (%)[a]	EC$_{50}$/nM[b]	T_m/°C[c]	Recovery (%)[a]	EC$_{50}$/nM[b]	T_m/°C[c]
HIV$_{V38A}$						
Ser	11.8	1.1 ± 0.3	72.6	9.3	3.4 ± 1.4	60.0
Ala	11.4	0.7 ± 0.2	76.1	10.0	2.2 ± 0.8	64.6
Leu	10.3[d]	0.8 ± 0.1	75.0	10.1[d]	3.4 ± 1.6	57.5
Pro	0.4	340 ± 61	56.3	0.0	>1000	49.7
Thr	10.8	0.8 ± 0.1	70.4	8.1	28 ± 12	57.8
Trp	1.0	22 ± 5.6	64.6	7.7	>1000	53.2
HIV$_{N43D}$						
Ser	10.9	0.3 ± 0.1	69.9	7.4	2.0 ± 0.4	65.3
Ala	12.9	0.2 ± 0.1	74.4	10.2	0.3 ± 0.1	71.9
Leu	12.9[d]	0.2 ± 0.1	80.0	10.8[d]	0.2 ± 0.1	74.0
Pro	0.3	130 ± 52	55.6	0.3	430 ± 160	55.0
Thr	9.4	0.3 ± 0.1	67.5	6.1	3.7 ± 0.1	62.4
Trp	2.4	2.7 ± 0.6	66.0	7.6	220 ±17	61.4

[a] The recovery rate was determined from the relative detected signals of [M + 3H]$^{3+}$ and [M + 4H]$^{4+}$ ions by LC-MS analysis. [b] EC$_{50}$ was determined as the concentration that blocked HIV-1$_{NL4-3}$ replication by 50% in the MAGI assay. To improve the replication kinetics, the D36G mutation, observed in the majority of HIV-1 strains, was introduced into the NL4-3 background used in this study. [c] T_m values were defined by the midpoint of the thermal unfolding transition state measured by monitoring the molar ellipticity at 222 nm of N36$_{V38A}$/SC35EK$_{S138X}$, N36$_{N43D}$/SC35EK$_{S138X}$, N54$_{V38A}$/T-20EK$_{S138X}$ or N54$_{N43D}$/T-20EK$_{S138X}$ mixture. [d] Combined yield of 138I and 138L derivatives.

relationship of T-20EK$_{S138X}$ can be partially rationalized by the similar hydrophobic/hydrophilic properties of the side-chain. The recovery rates of T-20EK$_{S138X}$ in affinity selection showed good correlations with both anti-HIV activity and with thermal stability of the complexes (Fig. 3c and 3d). The peptides captured with more than 9% recovery yields exhibited sub-nanomolar potency along with T_m values >75 °C.

The anti-HIV activities of the series of peptides against recombinant viruses with either the enfuvirtide-resistant V38A or N43D mutation in N-HR were evaluated. The results of representative C-HR peptides, which were obtained by a single nucleotide mutation of HIV-1$_{NL4-3}$, are shown in Table 3 and Figure S2.† From Ser138 encoded by the TCG codon in wild-type NL4-3, Ala (GCG), Pro (CCG), Thr (ACG), Leu (TTG) and Trp (TGG) are possible mutations; the other mutations are silent (TCA, TCT, TCC) or a stop codon (TAG). The S138A substitution in both SC35EK and T-20EK enhanced the thermal

stability of the N-HR/C-HR complex, indicating that this is a favorable mutation in terms of gp41 folding of the resistant virus.[3,4] These peptides by mutant-directed design restored and enhanced the anti-HIV activity against enfuvirtide-resistant variants. The S138L peptide was also effective against both V38A and N43D strains; however, no emergence of a clinical variant having this mutation has been reported. Of interest, resistant viruses are unlikely to necessarily use the best C-HR substitution to complement the gp41 folding, presumably due to the low replication kinetics. These results indicate that the mutations observed in clinical variants can direct the position to be optimized for inhibitor design but not the most appropriate amino acids. In practice, several other substitutions by Ile and Met, which are irrelevant to single nucleotide mutations from the wild-type, also provided potent anti-HIV activity against the resistant strains (Table S4, ESI†). In contrast, substitution with Pro or Trp for both peptides significantly decreased the activity,

This journal is © The Royal Society of Chemistry 2010

Med. Chem. Commun., 2010, **1**, 276–281 | 279

Table 4 Peptide recovery in affinity selection, anti-HIV activity and thermal stability of the six-helix bundles of SC35EK$_{Q141X}$ and T-20EK$_{Q141X}$ derivatives

X	SC35EK$_{Q141X}$			T-20EK$_{Q141X}$		
	Recovery (%)[a]	EC$_{50}$/nM[b]	T_m/°C[c]	Recovery (%)[a]	EC$_{50}$/nM[b]	T_m/°C[c]
Gln	10.1	2.6 ± 0.3	81.6	8.2[e]	1.5 ± 0.6	78.8
Ala	6.6	1.6 ± 0.6	76.1	5.6	2.7 ± 0.3	70.4
Asp	4.5	2.9 ± 0.1	75.1	8.2	3.5 ± 0.7	71.4
Glu	4.3	2.4 ± 0.4	76.2	8.2[e]	3.8 ± 0.8	71.8
Phe	5.7	2.6 ± 0.4	76.7	5.3	2.6 ± 0.9	64.0
Gly	3.8	2.3 ± 0.7	71.0	3.4	3.0 ± 0.6	66.2
His	4.3	2.0 ± 0.5	72.6	3.7	3.0 ± 0.6	68.4
Ile	8.2[d]	2.9 ± 0.4	79.7	10.4[d]	0.8 ± 0.3	74.0
Lys	4.8	2.7 ± 0.5	69.2	4.8	3.8 ± 0.3	65.3
Leu	8.2[d]	2.7 ± 0.9	83.8	10.4[d]	0.5 ± 0.2	77.4
Met	6.0	2.0 ± 0.3	80.2	9.2	0.9 ± 0.1	74.6
Asn	4.0	2.5 ± 0.5	73.4	4.4	3.6 ± 0.7	69.0
Pro	0.0	58 ± 16	60.2	0.3	>1000	52.0
Arg	7.6	2.5 ± 0.1	71.5	7.2	1.5 ± 0.3	68.9
Ser	4.0	2.5 ± 0.7	72.4	3.2	4.6 ± 1.4	66.7
Thr	7.3	3.2 ± 0.6	76.7	6.9	2.1 ± 0.5	71.6
Val	6.2	2.2 ± 0.6	77.7	6.1	2.9 ± 0.2	70.5
Trp	7.1	1.7 ± 0.2	77.1	8.1	2.5 ± 0.1	68.8
Tyr	5.5	2.2 ± 0.6	76.3	4.9	2.3 ± 0.9	67.7

[a] The recovery rate was determined from the relative detected signals of [M + 3H]$^{3+}$ and [M + 4H]$^{4+}$ ions by LC-MS analysis. [b] EC$_{50}$ was determined as the concentration that blocked HIV-1$_{NL4-3}$ replication by 50% in the MAGI assay. To improve the replication kinetics, the D36G mutation, observed in the majority of HIV-1 strains, was introduced into the NL4-3 background used in this study. [c] T_m values were defined by the midpoint of the thermal unfolding transition state measured by monitoring the molar ellipticity at 222 nm of N36/SC35EK$_{Q141}$ or N54/T-20EK$_{Q141}$ mixture. [d] Combined yield of 141I and 141L derivatives. [e] Combined yield of 141E and 141Q derivatives.

which is consistent with the results against the wild-type virus. Lower stabilities of the six-helical bundle structure consisting of S138T peptides and mutant N-HR peptides were shown, but SC35EK$_{S138T}$ was slightly more potent against both resistant viruses compared with the parent peptide.

Using His-tagged N36 or N54 peptides with the V38A or N43D mutation, affinity selection experiments were performed for SC35EK$_{S138X}$ and T-20EK$_{S138X}$ including 19 components (Table 3 and Table S4, ESI†). Eight SC35EK derivatives captured in significantly high yields all showed potent anti-HIV activity against the V38A mutant. Moderate recovery yields of SC35EK$_{S138E}$ and SC35EK$_{S138Y}$ could result from potential false positive and negative results of the selection, respectively. Although T-20EK derivatives showed lower susceptibility against the V38A mutant in the MAGI assay, an association between the high recovery rate and more potent anti-HIV activity was observed such as S138A, S138I, S138L and S138M derivatives (Figures S3, ESI†). Similar correlations were also obtained against N43D variants. SC35EK$_{S138X}$ and T-20EK$_{S138X}$ components, which exhibited subnanomolar potent bioactivity, were recovered in moderate to good yields. Overall favorable amino acids for position 138 of the wild-type were useful for designing C-HR peptides against V38A and N43D variants and *vice versa*, suggesting that the essential binding mode around this position is conserved even after acquiring the enfuvirtide resistance.

The structure–activity relationships of Q141 modifications were also investigated (Table 4). All SC35EK$_{Q141X}$ and T-20EK$_{Q141X}$ peptides except for the Q141P substitution exhibited similar anti-HIV activity in the EC$_{50}$ range of 1.6–3.2 nM and 0.51–4.6 nM, respectively. The significantly low T_m values of Q141P derivatives suggested that the sole proline

residue precluded the formation of a bioactive α-helix structure. On the other hand, high potency of the other peptides independent of any other acyclic amino acid substitution at position 141 may be attributable to the lower importance of the Q141 position for the binding affinity between N-HR and C-HR than the S138 position. Among these, Q141I, Q141L and Q141M peptides formed slightly more stable complexes with N36 or N54 and were captured at a relatively higher recovery rate by affinity selection. These substitutions were found to contribute to subnanomolar anti-HIV activity of T-20EK derivatives; however, these peptides were less valid for SC35EK derivatives.

For both S138 and Q141 substitutions, it does not seem possible to distinguish between variations of a few nM in anti-HIV activity by affinity selection. This is particularly the case for the selections regarding less effective residues such as Q141 of SC35EK. In contrast, over a larger range of more than 2 orders of magnitude of affinity variations of T-20EK derivatives, the selection procedure correlated reasonably well with the anti-HIV activity and six-helix bundle stability. In both sequences, highly potent anti-HIV activity peptides were captured in good to high yields.

Conclusions

In conclusion, we have presented an affinity selection-mass spectrometry method to explore novel HIV-1 fusion inhibitors. Predicated on previous findings that the introduction of α-helix-inducible X-EE-XX-KK motifs into inhibitory C-HR peptides should improve peptide solubility in aqueous buffers and disclose the interactive surface to be optimized, a pool of SC35EK and T-20EK derivatives with a single modification at two interactive positions were screened using N-HR peptides corresponding to

wild-type and enfuvirtide-resistant strains. Through the screening of position 138 on C-HR, it was demonstrated that potent anti-HIV peptides could be obtained by substitutions with resistance-related and resistance-independent amino acids. Since a wide variety of synthetic peptides with any unnatural amino acids or peptidomimetics could be employed as candidate components, the system should be applicable to screening for inhibitory α-helix peptides of coiled-coil interactions. The structure–activity relationships of C-HR peptides presented herein may also be suitable in the design of the next-generation of fusion inhibitors. Additionally, since this process is considered to reproduce the evolutionary process of HIV-1 gp41 to select the appropriate folding partners in the presence of fusion inhibitors, the sequence-activity relationships could facilitate understanding of the underlying mechanisms of enfuvirtide resistance.

Acknowledgements

References

1 T. Matthews, M. Salgo, M. Greenberg, J. Chung, R. DeMasi and D. Bolognesi, *Nat. Rev. Drug Discovery*, 2004, **3**, 215–225.
2 D. C. Chan, C. T. Chutkowski and P. S. Kim, *Proc. Natl. Acad. Sci. U. S. A.*, 1998, **95**, 15613–15617.
3 L. Xu, A. Pozniak, A. Wildfire, S. A. Stanfield-Oakley, S. M. Mosier, D. Ratcliffe, J. Workman, A. Joall, R. Myers, E. Smit, P. A. Cane, M. L. Greenberg and D. Pillay, *Antimicrob. Agents Chemother.*, 2005, **49**, 1113–1119.
4 L. Pérez-Alvarez, R. Carmona, A. Ocampo, A. Asorey, C. Miralles, S. Pérez de Castro, M. Pinilla, G. Contreras, J. A. Taboada and R. Nájera, *J. Med. Virol.*, 2006, **78**, 141–147.
5 D. Eggink, J. P. Langedijk, A. M. Bonvin, Y. Deng, M. Lu, B. Berkhout and R. W. Sanders, *J. Biol. Chem.*, 2009, **284**, 26941–26950.
6 D. Nameki, E. Kodama, M. Ikeuchi, N. Mabuchi, A. Otaka, H. Tamamura, M. Ohno, N. Fujii and M. Matsuoka, *J. Virol.*, 2005, **79**, 764–770.
7 D. C. Chan, D. Fass, J. M. Berger and P. S. Kim, Core structure of gp41 from the HIV envelope glycoprotein, *Cell*, 1997, **89**, 263–273.
8 T. Watabe, Y. Terakawa, K. Watanabe, H. Ohno, H. Nakano, T. Nakatsu, H. Kato, K. Izumi, E. Kodama, M. Matsuoka, K. Kitaura, S. Oishi and N. Fujii, *J. Mol. Biol.*, 2009, **392**, 657–665.
9 K. Izumi, S. Nakamura, H. Nakano, K. Shimura, Y. Sakagami, S. Oishi, S. Uchiyama, T. Ohkubo, Y. Kobayashi, N. Fujii, M. Matsuoka and E. N. Kodama, *Antiviral Res.*, 2010, **87**, 179–186.
10 J. P. Lalezari, N. C. Bellos, K. Sathasivam, G. J. Richmond, C. J. Cohen, R. A. Myers, Jr., D. H. Henry, C. Raskino, T. Melby, H. Murchison, Y. Zhang, R. Spence, M. L. Greenberg, R. A. Demasi and G. D. Miralles, *J. Infect. Dis.*, 2005, **191**, 1155–1163.
11 Y. He, Y. Xiao, H. Song, Q. Liang, D. Ju, X. Chen, H. Lu, W. Jing, S. Jiang and L. Zhang, *J. Biol. Chem.*, 2008, **283**, 11126–11134.
12 K. Izumi, E. Kodama, K. Shimura, Y. Sakagami, K. Watanabe, S. Ito, T. Watabe, Y. Terakawa, H. Nishikawa, S. G. Sarafianos, K. Kitaura, S. Oishi, N. Fujii and M. Matsuoka, *J. Biol. Chem.*, 2008, **284**, 4914–4920.
13 J. Cao, L. Bergeron, E. Helseth, M. Thali, H. Repke and J. Sodroski, *J. Virol.*, 1993, **67**, 2747–2755.
14 W. Shu, J. Liu, H. Ji, L. Radigen, S. Jiang and M. Lu, *Biochemistry*, 2000, **39**, 1634–1642.
15 D. A. Annis, N. Nazef, C. C. Chuang, M. P. Scott and H. M. Nash, *J. Am. Chem. Soc.*, 2004, **126**, 15495–15503.
16 G. C. Adam, C. A. Parish, D. Wisniewski, J. Meng, K. Liu, K. Calati, B. D. Stein, J. Athanasopoulos, P. Liberator, T. Roemer, G. Harris and K. T. Chapman, *J. Am. Chem. Soc.*, 2008, **130**, 16704–16710.
17 S. Oishi, S. Ito, H. Nishikawa, K. Watanabe, M. Tanaka, H. Ohno, K. Izumi, Y. Sakagami, E. Kodama, M. Matsuoka and N. Fujii, *J. Med. Chem.*, 2008, **51**, 388–391.
18 A. Otaka, M. Nakamura, D. Nameki, E. Kodama, S. Uchiyama, S. Nakamura, H. Nakano, H. Tamamura, Y. Kobayashi, M. Matsuoka and N. Fujii, *Angew. Chem., Int. Ed.*, 2002, **41**, 2937–2940.
19 M. Gochin, R. Savage, S. Hinckley and L. Cai, *Biol. Chem.*, 2006, **387**, 477–483.
20 H. Nishikawa, E. Kodama, A. Sakakibara, A. Fukudome, K. Izumi, S. Oishi, N. Fujii and M. Matsuoka, *Antiviral Res.*, 2008, **80**, 71–76.
21 J. K. Judice, J. Y. Tom, W. Huang, T. Wrin, J. Vennari, C. J. Petropoulos and R. S. McDowell, *Proc. Natl. Acad. Sci. U. S. A.*, 1997, **94**, 13426–13430.
22 S. K. Sia, P. A. Carr, A. G. Cochran, V. N. Malashkevich and P. S. Kim, *Proc. Natl. Acad. Sci. U. S. A.*, 2002, **99**, 14664–14669.
23 J. J. Dwyer, K. L. Wilson, D. K. Davison, S. A. Freel, J. E. Seedorff, S. A. Wring, N. A. Tvermoes, T. J. Matthews, M. L. Greenberg and M. K. Delmedico, *Proc. Natl. Acad. Sci. U. S. A.*, 2007, **104**, 12772–12777.

This journal is © The Royal Society of Chemistry 2010

Med. Chem. Commun., 2010, 1, 276–281 | 281

−84−

Article

The Essential Functions of Adipo-osteogenic Progenitors as the Hematopoietic Stem and Progenitor Cell Niche

Yoshiki Omatsu,[1] Tatsuki Sugiyama,[1] Hiroshi Kohara,[1] Gen Kondoh,[2] Nobutaka Fujii,[3] Kenji Kohno,[4] and Takashi Nagasawa[1,*]

[1]Department of Immunobiology and Hematology
[2]Laboratory of Animal Experiments for Regeneration, Institute for Frontier Medical Sciences
Kyoto University, 53 Kawahara-cho, Shogoin, Sakyo-ku, Kyoto 606-8507, Japan
[3]Graduate School of Pharmaceutical Sciences, Kyoto University, Sakyo-ku, Kyoto 606-8501, Japan
[4]Laboratory of Molecular and Cell Genetics, Graduate School of Biological Sciences, Nara Institute of Science and Technology (NAIST),
8916-5 Takayama, Ikoma, Nara 630-0192, Japan
*Correspondence: tnagasa@frontier.kyoto-u.ac.jp
DOI 10.1016/j.immuni.2010.08.017

SUMMARY

Hematopoietic stem cells (HSCs) and their lympho-hematopoietic progeny are supported by microenvironmental niches within bone marrow; however, the identity, nature, and function of these niches remain unclear. Short-term ablation of CXC chemokine ligand (CXCL)12-abundant reticular (CAR) cells in vivo did not affect the candidate niches, bone-lining osteoblasts, or endothelial cells but severely impaired the adipogenic and osteogenic differentiation potential of marrow cells and production of the cytokines SCF and CXCL12 and led to a marked reduction in cycling lymphoid and erythroid progenitors. HSCs from CAR cell-depleted mice were reduced in number and cell size, were more quiescent, and had increased expression of early myeloid selector genes, similar to the phenotype of wild-type HSCs cultured without a niche. Thus, the niche composed of adipo-osteogenic progenitors is required for proliferation of HSCs and lymphoid and erythroid progenitors, as well as maintenance of HSCs in an undifferentiated state.

INTRODUCTION

Hematopoietic stem cells (HSCs) give rise to all lineages of blood cells, including immune cells in the bone marrow. It has been assumed that the special microenvironments known as niches play an essential role in maintaining HSCs and hematopoietic progenitors in the marrow to provide appropriate numbers of mature blood cells throughout life (Morrison and Spradling, 2008; Wilson and Trumpp, 2006). HSCs and lymphoid progenitors are thought to reside in their niches, and the identity of the niche has been a subject of longstanding debate. It has been shown that HSCs are in contact with a population of osteoblasts lining the bone surface, termed spindle-shaped N-cadherin$^+$CD45$^-$ osteoblastic (SNO) cells, which express

a high amount of N-cadherin (endosteal niches) (Zhang et al., 2003). In contrast, many HSCs are associated with sinusoidal endothelium, suggesting that endothelial cells create cellular niches for HSCs (vascular niches) (Kiel et al., 2005). We have shown that CXCR4, a primary receptor for the CXC chemokine ligand (CXCL)12 (also known as stromal cell-derived factor-1) (Nagasawa, 2006; Nagasawa et al., 1996; Nagasawa et al., 1994; Tachibana et al., 1998; Zou et al., 1998), is essential for maintaining a pool of HSCs and B cells and that most HSCs, early B cell precursors, and plasma cells are scattered throughout the bone marrow cavity and are in contact with a small population of reticular cells with long processes, expressing high amounts of CXCL12, called CXCL12-abundant reticular (CAR) cells, suggesting that CAR cells are a key component of niches for both HSCs and B cells (Nagasawa, 2008; Sugiyama et al., 2006; Tokoyoda et al., 2004). However, these studies do not reveal the functions of SNO cells, endothelial cells, and CAR cells as niches for HSCs and/or lymphoid progenitors.

Prior studies using a variety of gain-of-function and loss-of-function approaches examined the identity and functions of cellular niches for HSCs and hematopoietic progenitors. Bone morphogenetic protein (BMP) receptor type IA (BMPRIA) conditionally deficient mice displayed increases in the numbers of SNO cells, which correlated with an increase in the numbers of HSCs (Zhang et al., 2003). Parathyroid hormone (PTH) administration increased the numbers of osteoblasts in culture and induced an increase in the number of HSCs in vivo (Calvi et al., 2003). In contrast, it has been shown that depleting osteoblastic lineage cells with a 2.3 kb fragment from the rat type I collagen α1 (Col1α1) gene promoter driving thymidine kinase (Col2.3ΔTK) induced a marked reduction in hematopoietic cells (Visnjic et al., 2004; Zhu et al., 2007). These results suggest that osteoblastic lineage cells maintain HSCs and hematopoietic cells but do not rule out the possibility that Col1α1, BMPRIA, and PTH or PTH-related protein receptor (PPR) are expressed in bone marrow reticular cells, including CAR cells. In addition, it has been reported that reductions in osteoblasts do not necessarily lead to reductions in HSCs and hematopoietic cells (Kiel et al., 2007; Wilson and Trumpp, 2006). Together, it remains unresolved which cell types play major roles in regulating the

maintenance of HSCs and lymphoid progenitors within bone marrow.

It is assumed that most adult HSCs are quiescent and that HSC quiescence is maintained by their niches (Arai et al., 2004; Orford and Scadden, 2008). In contrast, many studies have shown that the majority of HSCs are cycling, albeit slowly, although some HSCs are highly dormant, (Cheshier et al., 1999; Foudi et al., 2009; Santaguida et al., 2009; Wilson et al., 2008; Yamazaki et al., 2006) and that many lineage-restricted progenitors are known to be cycling actively, supporting the idea that HSC and hematopoietic progenitor proliferation is maintained by their niches. However, the technology to prove this was lacking and the role of niches in controlling the quiescence, proliferation, and differentiation of HSCs and lymphoid progenitors remain unclear. Here, we generated mice that allow selective ablation of CAR cells in bone marrow and determined the nature and in vivo function of CAR cells as a niche for HSCs and lympho-hematopoietic progenitors.

RESULTS

Generation of Mice that Allow Inducible Selective Ablation of CAR Cells In Vivo

To determine the nature and in vivo function of CAR cells, we generated mice in which a transgene encoding the Diphtheria toxin (DT) receptor-green fluorescent protein (DTR-GFP) fusion protein (Saito et al., 2001) was knocked into the *Cxcl12* locus (CXCL12-DTR-GFP mice) (Figure 1A). These mice allow the conditional ablation of CXCL12-expressing cells by DT administration because wild-type murine cells are insensitive to killing by DT (Saito et al., 2001). CXCL12-DTR-GFP mice were injected intraperitoneally (i.p.) with DT at a dose of 25 ng/kg; many mice remained healthy for up to 3 days after injection and died 5 days after injection probably from liver failure. By histological analysis, the liver of CXCL12-DTR-GFP mice showed necrosis and haemorrhage at 5 days after DT treatment but appeared normal at 2 days after DT treatment. Histological analysis of bone marrow microenvironments 2 or 3 days after DT treatment revealed that CXCL12-DTR-GFP+ CAR cells were eliminated or severely reduced, but bone-lining SNO cells, osteocalcin+ or marked alkaline phosphatase (ALP) activity-containing osteoblasts, and sinusoidal endothelial cells remained unaffected in DT-treated CXCL12-DTR-GFP mice compared with untreated CXCL12-DTR-GFP mice (Figures 1B and 1C; Figure S1 available online; data not shown). Flow-cytometric analysis confirmed that the numbers of CXCL12-DTR-GFPhi CAR cells were severely reduced in DT-treated CXCL12-DTR-GFP mice compared with untreated animals (Figure 1E). In addition, consistent with the result that CAR cells are a small population of VCAM-1+ reticular cells (Tokoyoda et al., 2004), many VCAM-1+ reticular cells were observed in DT-treated and untreated CXCL12-DTR-GFP mice (Figure 1D).

Short-Term Ablation of CAR Cells Leads to a Reduction in Cycling Lymphoid and Erythroid Progenitors

To better define the direct effect of CAR cell depletion on hematopoiesis, we examined the effect of short-term ablation of CAR cells on hematopoietic cells in the bone marrow using CXCL12-DTR-GFP mice 2 days after DT treatment, in which CAR cells were eliminated or severely reduced. Total bone marrow cellularity was reduced in DT-treated CXCL12-DTR-GFP mice compared with DT-treated and untreated wild-type mice (Figure 2A and Figure S2A). Flow-cytometric analysis of hematopoietic progenitors revealed that although the numbers of Lineage(Lin)−Sca-1+c-kit+Flt3+ multipotent progenitors (MPPs) (Adolfsson et al., 2001) appeared normal, Lin−IL-7Rα+Flt3+ common lymphoid progenitors (CLPs) (Karsunky et al., 2008) and c-kit+CD71+Ter119lo proerythroblasts were almost absent, the numbers of c-kit+CD19+IgM− pro-B cells and Lin−Sca-1−c-kit+CD34−FcγRII-IIIlo megakaryocyte and erythrocyte progenitors (MEPs) (Akashi et al., 2000) were severely reduced and the number of Lin−Sca-1−c-kit+CD34+FcγRII-IIIhi granulocyte and macrophage progenitors (GMPs) (Akashi et al., 2000) was more modestly reduced in DT-treated CXCL12-DTR-GFP mice compared with untreated CXCL12-DTR-GFP mice or DT-treated and untreated wild-type mice (Figures 2B and 2C and Figure S2A). Cell-cycle analysis of pro-B cells and MEPs using Pyronin Y (PY) revealed that around half of the cells were cycling actively (high PY fluorescence [PYhi]) and other quiescent cells displayed low PY fluorescence (PYlo) in DT-treated wild-type mice. In contrast, a reduction in the frequency of PYhi cells and an increase in the frequency of PYlo cells were observed in DT-treated CXCL12-DTR-GFP mice (Figure 2D). Additionally, Annexin-V staining of pro-B cells revealed many apoptotic cells (43%) in DT-treated CXCL12-DTR-GFP mice although few (5.1%) were detected in DT-treated wild-type mice (Figure 2E). These results indicate that CAR cells are essential for lymphoid, erythroid, and myeloid lineage development and suggest that CAR cells support the survival and proliferation of B cell progenitors and proliferation of erythroid progenitors.

HSCs Are Reduced and More Quiescent in the Absence of CAR Cells

We next examined the effect of short-term ablation of CAR cells on HSCs. Bone marrow from CXCL12-DTR-GFP and wild-type mice was analyzed 2 days after DT treatment. The number of CD34−Lin−Sca-1+c-kit+CD150+CD48− cells, which are highly enriched for long-term repopulating HSCs (Foudi et al., 2009; Kiel et al., 2005; Wilson et al., 2008), was reduced, but to a lesser extent than lymphoid and erythroid progenitors in DT-treated CXCL12-DTR-GFP mice compared with control animals (Figure 3A and Figure S3A). Because the unambiguous measure of HSCs is long-term transplantation, we estimated the numbers of HSCs using repopulating units (RU), based on a competitive repopulation assay (Harrison et al., 1993). The numbers of RU were reduced about 50% in the bone marrow of CXCL12-DTR-GFP mice compared with wild-type mice (Figure 3B), indicating that CAR cells play an essential role in maintaining the HSC number.

Flow-cytometric analysis using the proliferation marker Ki67 has shown that a small percentage of CD34−Lin−Sca-1+c-kit+CD48− HSCs express Ki67 in DT-treated or untreated wild-type mice, as reported previously, but the numbers of Ki67-positive cells were severely reduced in the HSC population from DT-treated CXCL12-DTR-GFP mice (Figure 3C). Quantitative, real-time polymerase chain reaction with reverse transcription (qRT-PCR) analysis revealed that the mRNA expression of Evi-1 and Pbx1, which are essential for HSC maintenance and
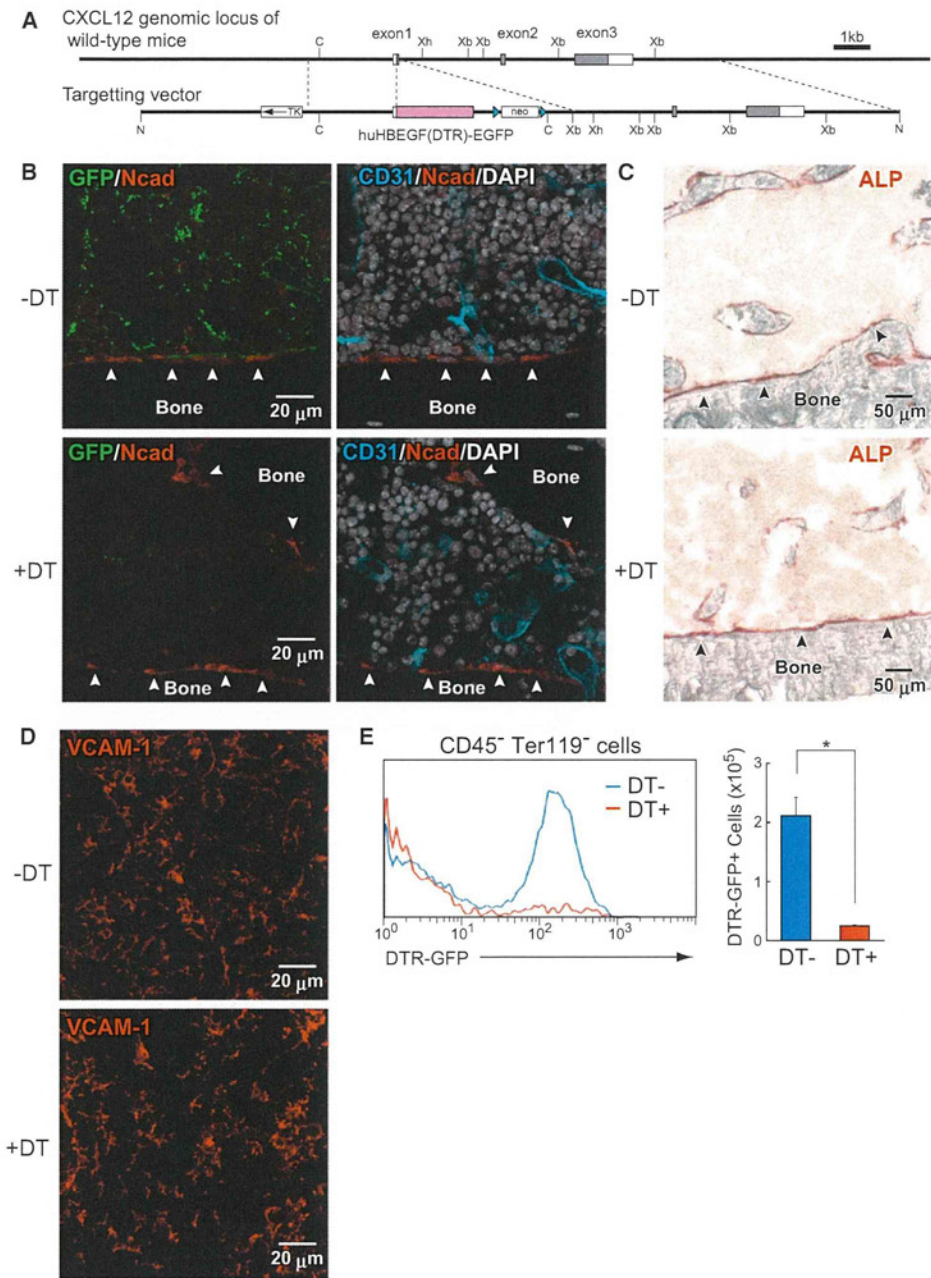
Figure 1. Short-Term Selective Ablation of CAR Cells In Vivo in Bone Marrow

(A) Strategy used to generate CXCL12-DTR-GFP mice. C, Csp45I; Xh, XhoI; Xb, XbaI; N, NotI. Triangles represent LoxP sites.

(B–E) Bone marrow from CXCL12-DTR-GFP mice was analyzed 2 days after administration of DT or control vehicle. Bone marrow sections were stained with antibodies against GFP, N-cadherin, the panendothelial marker PECAM-1 (CD31) (B), and VCAM-1 (D) and assayed by Fast Red staining (C). CXCL12-DTR-GFP+ CAR cells (green) are eliminated (B, left); however, bone-lining SNO cells detected by anti-N-cadherin antibodies (B, arrowheads; red), marked ALP activity-containing osteoblasts (C, arrowheads; red), and sinusoidal endothelial cells (B, right; blue) exhibit normal numbers and morphology in DT-treated CXCL12-DTR-GFP mice. The nuclei of cells were labeled with DAPI dye (B, right; white). (E) Flow cytometric analysis of CD45⁻Ter119⁻CD31⁻ nonhematopoietic cells. The numbers of CXCL12-DTR-GFPhi CAR cells per two femurs and tibiae are shown (E, right). All error bars represent SD of the mean. n = 4; *p < 0.05.

preferentially expressed in HSCs (Ficara et al., 2008; Goyama et al., 2008), was largely unaffected in the HSC population from DT-treated CXCL12-DTR-GFP mice (Figure 3D and Figure S3C). In contrast, although cell-cycle-promoting genes, including those that encode Cyclin D1, D2, A2, and their catalytic partner, Cdc2a, and a regulator of initiation of DNA replication, Cdc6, were expressed in the HSC population from DT-treated and untreated wild-type mice and untreated CXCL12-DTR-GFP
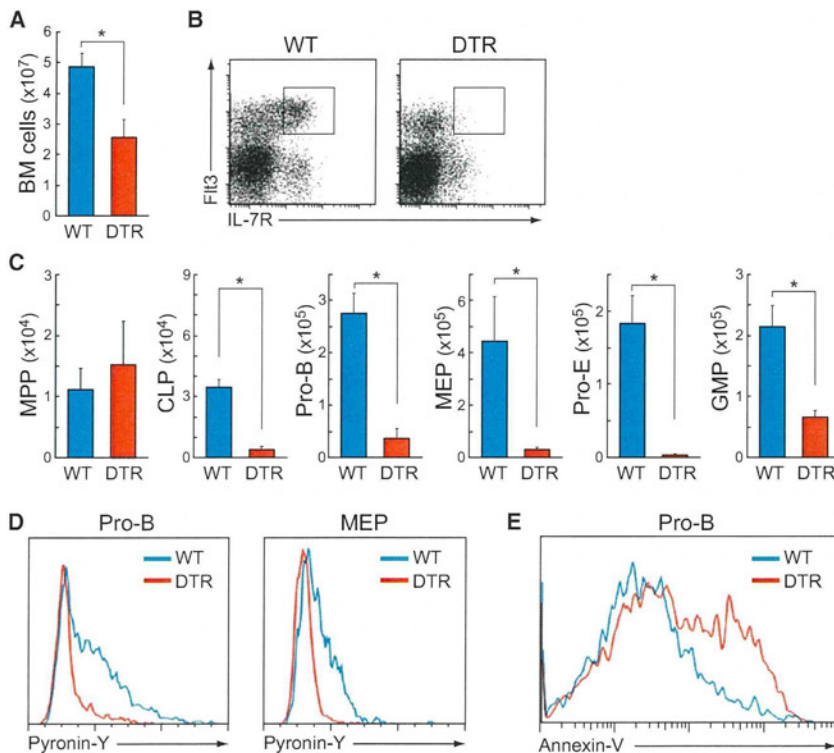
Figure 2. Essential In Vivo Functional Roles of CAR Cells in Lympho-hematopoietic Progenitors

Bone marrow from wild-type and CXCL12-DTR-GFP mice was analyzed by flow cytometry 2 days after DT administration.

(A) Total numbers of CD45$^+$ hematopoietic cells per two femurs and tibiae. n = 3; *p < 0.05.

(B) Immunofluorescent profiles of CLPs. Gated Lin$^-$ cells are analyzed for the expression of IL-7Rα and Flt3.

(C) The numbers of MPPs, CLPs, pro-B cells, MEPs, proerythroblasts (pro-E), and GMPs per two femurs and tibiae. n = 3; *p < 0.05.

(D) RNA content of pro-B cells and MEPs by PY staining.

(E) Annexin-V staining of pro-B cells.

All error bars represent SD of the mean (A and C).

Together, these results indicate that HSCs are more quiescent in CAR cell-depleted mice and that CAR cells keep HSCs in a proliferative state.

Short-Term Ablation of CAR Cells Induces Early Myeloid Differentiation of HSCs

It is unclear whether HSC niches regulate the differentiation of HSCs. To address this issue, we analyzed the expression of genes that encode activities important for HSC differentiation in the HSC population from CAR cell-depleted mice. It has been shown that elevating the expression of transcription factor PU.1 in primitive multipotent progenitors induces the generation of myeloid lineage (Arinobu et al., 2007; DeKoter and Singh, 2000). Of note, qRT-PCR analysis revealed that the mRNA expression of PU.1 and its macrophage-specific target M-CSF receptor (M-CSFR) was markedly increased in the CD34$^-$Lin$^-$Sca-1$^+$c-kit$^+$CD150$^+$ CD48$^-$ HSC population from CXCL12-DTR-GFP mice 2 days after DT treatment, compared with untreated CXCL12-DTR-GFP mice or DT-treated and untreated wild-type mice (Figure 3I and data not shown).

Cells in the HSC population were sorted from bone marrow of wild-type and CXCL12-DTR-GFP mice 2 days after DT treatment and cultured in the presence of SCF and CXCL12, which support myeloid differentiation from HSCs and more mature multipotent progenitors. Flow-cytometric analysis showed that substantial numbers of Gr-1^{hi}CD11b$^+$ myeloid lineage cells were generated from wild-type HSCs at day 10 of culture and peaked at day 14 or later (data not shown). In contrast, cells in the HSC population from CAR cell-depleted mice had generated substantial numbers of Gr-1^{hi}CD11b$^+$ myeloid lineage cells earlier, day 7 of culture, and peaked at day 10, supporting the idea that some cells in the HSC population from CAR cell-depleted mice are more differentiated than in wild-type mice (Figure 3J and data not shown). Together, these results suggest that short-term CAR cell depletion prevented HSC maintenance in an undifferentiated state.

mice, consistent with previous studies (Kalaszczynska et al., 2009; Kozar et al., 2004; Santaguida et al., 2009; Yamazaki et al., 2006), expression of these genes was markedly reduced in the HSC population from DT-treated CXCL12-DTR-GFP mice (Figure 3D and data not shown). In addition, mRNA expression of the transcriptional repressor Mad1, considered to decrease cell size (Iritani et al., 2002) and inhibit HSC proliferation (Walkley et al., 2005), was significantly elevated in the HSC population from DT-treated CXCL12-DTR-GFP mice (Figure 3D). Cellular activation by growth factors induces entry into a phase of cell cycle characterized by initiation of transcription and accumulation of RNA, mainly in the form of ribosomal RNA, which can be measured by RNA-specific dyes, such as PY. As reported previously, almost all CD34$^-$Lin$^-$Sca-1$^+$ c-kit$^+$CD48$^-$ HSCs from DT-treated wild-type mice displayed low PY fluorescence (Figure 3E); however, PY fluorescence in many HSCs from DT-treated CXCL12-DTR-GFP mice decreased further compared with wild-type mice (Figure 3E). Furthermore, in DT-treated CXCL12-DTR-GFP mice, most cells in the HSC population were smaller than those in control animals, shown by forward scatter characteristics (FSCs) on flow cytometry, although Annexin-V staining revealed no increase in apoptotic cells in the population (Figure 3F and Figure S3D). Histological analysis of the bone marrow from DT-treated CXCL12-DTR-GFP mice, in which CAR cells were severely reduced, revealed that CD150$^+$CD48$^-$CD41$^-$ HSCs, which did not adjoin CAR cells, were significantly smaller than HSCs in contact with the processes of residual CAR cells, indicating that short-term ablation of CAR cells leads to a significant decrease in the cell size of adjacent HSCs (Figures 3G and 3H).